energies

MDPI

Article

Power Transformer Spatial Acoustic Radiation Characteristics Analysis under Multiple Operating Conditions

Liming Ying [1], Donghui Wang [1,*], Jinwei Wang [1], Guodong Wang [2], Xiaowen Wu [3] and Jiangtao Liu [4]

1 School of Electrical Engineering, Wuhan University, Wuhan 430072, China; lmying@whu.edu.cn (L.Y.); wjw0405@whu.edu.cn (J.W.)
2 State Grid Yantai Power Supply Company, Yantai 265199, China; gdwangwhu@163.com
3 State Grid Hunan Electric Power Corporation Research Institute, Changsha 410007, China; wxwwhu@163.com
4 Department of Physics and Electrical Engineering, Hubei University of Education, Wuhan 430205, China; Liu_jiangtao@whu.edu.cn
* Correspondence: eastsunshine87@126.com; Tel.: +86-158-273-36583

Received: 15 October 2017; Accepted: 18 December 2017; Published: 1 January 2018

Abstract: Spatial acoustic radiation characteristics analysis is the precondition of reducing the noise influence of outdoor power transformer while multi-physical field coupling method can be applied to quantify and reveal these acoustic characteristics of a running power transformer. In this study, based on the theoretical analysis about noise generation and dissemination process, an acoustic radiation model about oil-immersed power transformer was established and verified with field test data in time and frequency domain. Then, far-field analysis and directivity analysis were accomplished to characterize acoustic field of power transformer under multiple operating conditions. Finally, the acoustic radiation influence on potential surrounding buildings were analyzed and discussed. The visual results and conclusion provide acoustic guide for the optimal planning and design about both power substation and ambient buildings.

Keywords: power transformer; audible noise; multi-physical field coupling; multiple operating conditions; far-field analysis; directivity analysis; planning and design optimization

1. Introduction

Accompanied with the expansion of city, the urban power load is increasing gradually while the power substations, especially the 110 kV power substation, originally located in the outskirts are gradually surrounding by new buildings. Due to the power transformer noise may affect residents around in both physiological and psychological ways, interfering with basic activities such as sleep, rest, work, study, and communication [1,2], the noise emission levels are facing more stringent environmental noise standards [3]. Based on this, the theoretical method and practical measures about assessing power transformer noise levels and reducing the influence of noise has aroused general concern, which is especially noticed by the transformer manufacturers [4] and the operators of power grids [5].

The noise level of oil-immersed power transformer relates to the vibration amplitude of core and windings, the working condition of clamps and fasteners, correspondingly, the recent research about noise emission of power transformers are going ahead also from these points as the vibration mechanism of core and windings, the vibration and noise transmission process, and the establishment of the power transformer noise radiation model.

In the research of vibration mechanism, for the vibration mechanism of core and windings, magnetostriction caused by compressive stress in the rolling direction is the vibration source of the core [6] and displacements of laminated iron core and yoke are dominated by effects of magneto-static forces especially at overlaps of corners and T-joints [7]. On the other hand, the cores vibration also increased though the low-frequency load current harmonics acted on winding [8] while based on the accurate analysis on the vibration mechanisms of windings and vibration signals, fault types in transformer windings could be diagnosed [9].

For the vibration and noise transmission process, the insulation oil reduces the low frequency response of the core structure, while the online vibration of the transformer tank is affected by the features of the transmission path from the internal structure to the tank [10], the identification result of the power transformers' nonlinear vibration system, which is corresponding to the features of the transmission path, could be used in estimating the vibration waveform in time domain [11]. Outside the oil tank, implementation of passive or active noise control is the main aim of research on noise transmission process in air. For the passive noise control, the selection of sound absorbing material and the corresponding sound absorption structure design play crucial roles in noise absorptive capacity [12,13], while the active noise control effect is directly influenced by the control algorithm and the distribution mode of sound source array [14,15].

For the noise radiation model and noise level measurement about power transformer, the total load noise level is more easily affected by the high-order harmonics of the load current in comparing with the large fundamental load current component [16]. After introducing a new algorithm based on the reverse calculation method [17] or the corrections made of both ambient noise and sound wall reflections per the IEC (International Electrotechnical Commission) Standards [18], the accuracy of transformer noise measurements improves significantly. Moreover, from the manufacturer point of view, considering the low-frequency noise of electrical substation was always presented and noticed in daily lives of residents near the source [19], the structural optimization and low- or ultra-low-noise power transformers design by means of acoustic radiation model arouses designer's attention gradually [20], to meet the increasingly stringent environmental standards, the improved core assembling form [21], and even optimized cooling system arrangement form [22] are taken into account by manufacturers.

Based on the analysis above, with the measurement or model, most current researches focus on the mechanism of noise or vibration generation and transmission about single core or winding under the experimental condition for the purpose of optimizing the structure, design, or material selection, however, for security reasons, the omnidirectional acoustic field measurement is unreachable around a power transformer in running, which means that the spatial sound radiation characteristic of a power transformer on site and its noise influence surrounding buildings to be built is currently ambiguous. So the solution to this unfinished issue owns the guiding significance for transformer manufacturers, operators of power grids, and urban planners.

In this paper, based on the multi-physical field coupling method, the spatial acoustic radiation characteristics about an 110 kV oil-immersed transformer in running were revealed, and its influence on surrounding potential buildings were analyzed and discussed. The result could provide data support for audible noise reduction projects inside the power substation, and offer acoustic guides for optimizing the layout of urban space around the power substation.

2. Theory and Computational Model

Inside a power transformer, the primary windings create magnetic fluxes that induce current in secondary windings. During this energy transfer process, the magnetic fluxes would cause magnetostriction in the core which is made of magnetostrictive material, this forms regular vibrations and noise transferred to the tank through the insulation oil and fixed joints. At the same time, the current in the coils also creates Lorentz forces, causing vibrations and load noise transferred to the tank. As byproduct of the energy conversion process between electrical energy and magnetic energy, the

whole generation process about vibration and the noise of the power transformer is shown in Figure 1, and the core of this process could be described with the following three sets of coupling equations.

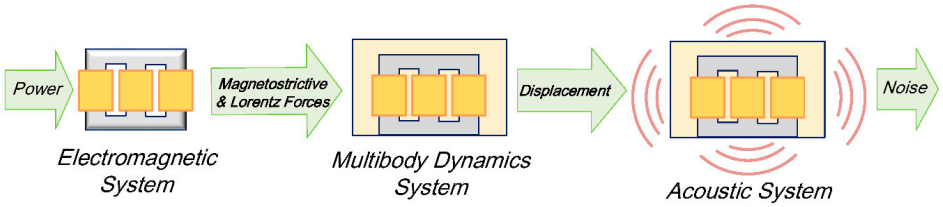

Figure 1. Generation process of vibration and noise.

2.1. Coupling Equations

According to the energy conversion process, three sets of coupling equations in this section respectively correspond with the electromagnetic coupling, electromagnetic-mechanical coupling and the mechanical-acoustic coupling.

The first is electromagnetic coupling. The current density inside the windings located within a time-varying but low-frequency magnetic field can be derived as:

$$\mathbf{J_e} = \frac{NI_{cir}}{S} \times \mathbf{e_{coil}}, \tag{1}$$

In this equation, N is the number of winding turns, I_{cir} is the coil current, S is the sectional area of a single turn, $\mathbf{e_{coil}}$ denotes the direction of electron flow.

Owing to the low frequency, after neglecting the displacement current, this partial differential equation can describe the electromagnetic process:

$$\sigma \frac{\partial \mathbf{A}}{\partial t} + \nabla \times (\frac{1}{\mu} \nabla \times \mathbf{A}) = \mathbf{J_e}, \tag{2}$$

This equation is derived from Maxwell's equations, where σ is the electric conductivity of the medium, μ is the differential permeability, $\mathbf{A}$ denotes the magnetic vector potential, and we can obtain the magnetic flux density with:

$$\mathbf{B} = \nabla \times \mathbf{A}, \tag{3}$$

Subsequently the electromagnetic-mechanical coupling is presented. Inside the power transformers under load, the magnetic stray-field of one current-carrying windings interact with the total current of the other windings, so that the main coupling between the magnetic field and the solid mechanical field is based on the Lorentz force. This electromagnetic force can be represented by the total current density $\mathbf{J}$ and the magnetic flux density $\mathbf{B}$:

$$\mathbf{f_V} = \mathbf{J} \times \mathbf{B}, \tag{4}$$

For the $\mathbf{J}$ in Equation (4), the term:

$$\sigma \mathbf{w} \times (\nabla \times \mathbf{A}), \tag{5}$$

should be added, which represents the induced eddy current density in the electrically conductive body moving with velocity $\mathbf{w}$ in a magnetic field, and this velocity $\mathbf{w}$ can be given as the time derivative of the mechanical displacement $\mathbf{d}$:

$$\mathbf{w} = \frac{\partial \mathbf{d}}{\partial t}, \tag{6}$$

The expression of total electric current density **J** is:

$$\mathbf{J} = -\sigma\frac{\partial \mathbf{A}}{\partial t} - \sigma\nabla V + \sigma\frac{\partial \mathbf{d}}{\partial t} \times (\nabla \times \mathbf{A}), \tag{7}$$

Based on the analysis above, substituting Equations (3) and (7) into Equation (4), the expression of magnetic volume force is obtained as shown in Equation (8):

$$\mathbf{f_V} = \mathbf{J} \times \mathbf{B} = [-\sigma\frac{\partial \mathbf{A}}{\partial t} - \sigma\nabla V + \sigma\frac{\partial \mathbf{d}}{\partial t} \times (\nabla \times \mathbf{A})] \times (\nabla \times \mathbf{A}), \tag{8}$$

The main coupling process of the magnetic field and the solid mechanical field can be described with this equation.

The third is mechanical-acoustic coupling. For the working condition of the power transformer, the speed of sound and density may in general be space-dependent, but only slowly varies with time. So, we can use the scalar wave equation to describe the changes of sound field induced by the vibration of the power transformer:

$$\frac{1}{\rho c^2}\frac{\partial^2 p_t}{\partial t^2} + \nabla(-\frac{1}{\rho}(\nabla p_t - \boldsymbol{q_d})) = \boldsymbol{Q_m}, \tag{9}$$

where p_t is the total acoustic pressure, ρ is the fluid density, c is the speed of sound, $\boldsymbol{q_d}$ is a domain volumetric force which represents a uniform constant background flow convecting the sound field, and $\boldsymbol{Q_m}$ is a domain source term, which represents a nonlinear contribution to the equations in the time domain.

For thin structures like oil tank walls with insulation oil and air on each side, the condition on exterior boundaries mathematically reads:

$$-\mathbf{n} \cdot \left(-\frac{1}{\rho}(\nabla p_t - \boldsymbol{q_d})\right) = -\mathbf{n} \cdot \mathbf{u_t}, \tag{10}$$

$$\mathbf{L_A} = p_t\mathbf{n}, \tag{11}$$

where $\mathbf{u_t}$ is the structural acceleration, $\mathbf{n}$ is the surface normal, and $\mathbf{L_A}$ is the load (force per unit area) experienced by the structure.

So, the acoustic load is given by the pressure drop across the thin structure, and this coupling includes the fluid load on the tank walls and the structural acceleration as experienced by the fluid.

2.2. Computational Model

After theoretical analysis about the generation process of vibration and noise, to visualize this process and apply it in a practical problem, a full-sized 3D acoustic radiation computational model of the power transformer was established in which both energy transmission paths from the core and windings to the air were considered:

In the first path, the coils' vibrations were transmitted to the oil tank through the fixture as well as from the magnetostriction, hence causing the tank to vibrate jointly. Then the audible noise in air was emitted.

In the second path, the noise in oil was produced by the vibration of both the core and the coils, then acted on the interior wall of oil tank and excited the vibration of the tank, afterward emitting noise in air.

Figure 2 presents the physical fields involved in these two paths, the type and main parameters of this natural oil circulation air cooling (ONAF) power transformer as illustrated in Figure 3a is shown in Table 1, COMSOL Multiphysics (Version 5.3, COMSOL Inc., Stockholm, Sweden) was selected as the main computing tool, and corresponding grids about key components inside oil tank were shown in Figure 3b.

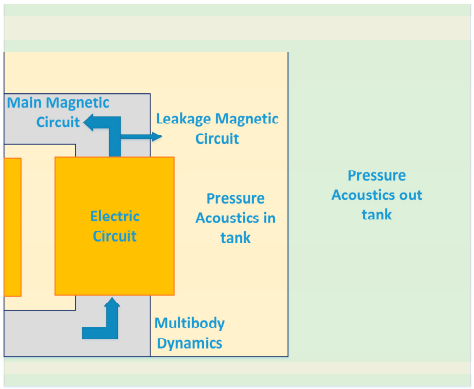

Figure 2. Sketch about physical fields.

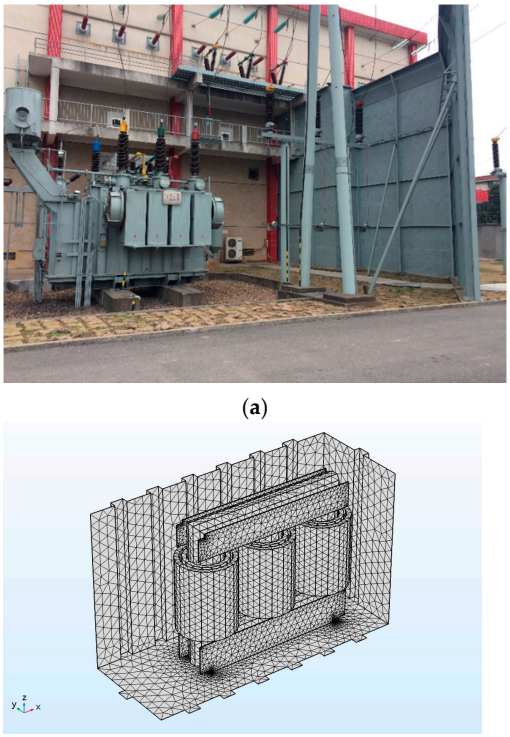

(**a**)

(**b**)

Figure 3. Photo of target transformer and grids: (**a**) Target transformer and site environment; (**b**) Grid.

Table 1. Main parameters of SFZ8-31500/110 transformer.

Operation Parameter	**Geometric Parameter (mm)**				
Rated frequency 50 Hz	Core	Length 2560	Height 2310	Diameter 500	
Rated capacity 31,500 kVA	Low-voltage winding	Inside diameter 560	Outside diameter 688	Height 1157	Turns 131
Rated voltage 110/10.5 kV	High-voltage winding	Inside diameter 762	Outside diameter 902	Height 1139	Turns 792
Short circuit impedance 13.26%	Tank	Length 4100	Width 1600	Height 2470	

3. Verification

To validate this spatial acoustic radiation model of power transformer built in Part 2, this model was located in an area outlined in Figure 4a, with the space, size, and material quality of the part boundaries about this area being consistent with the actual conditions shown in Figure 3a. The relative positions of the power transformer, microphones, and accelerometers from vertical view are shown in Figure 4b. The operating data shows three phase loads of this power transformer on site were balanced and phase current at high voltage side was 54 A, this means the load rate was 35% and high side currents in model were consistent with the actual situation.

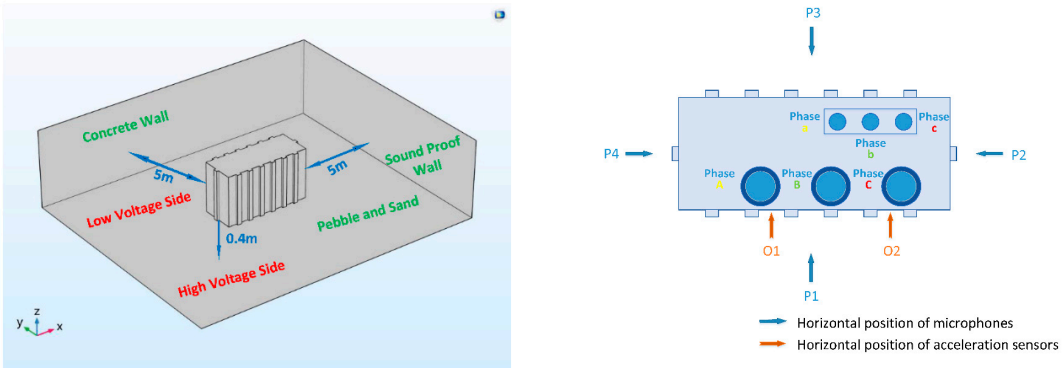

(**a**) (**b**)

Figure 4. Location of power transformer and microphones and acceleration sensors: (**a**) Location plan of power transformer; (**b**) Horizontal position of microphones and acceleration sensors.

3.1. Verification in Time Domain

In the time domain, the main validation index is the acceleration of the tank wall. The position of accelerometers at the high voltage side in site measurement are shown in Figure 4b as two orange arrows. Specifically, the height of the plane according to the accelerometers was 1230 mm, and these accelerometers were stuck on the tank wall. Then, the collected acceleration data within a certain period of time were compared with the calculated values at the same positions in this spatial acoustic radiation model. Table 2 shows the comparison between measured acceleration values and calculated stable acceleration values of the oil tank wall. The relative error values γ_a are calculated with the following formula:

$$\gamma_a = \frac{||c_a| - |\mu_a||}{|\mu_a|} \times 100\%, \tag{12}$$

where c_a is the calculated value and μ_a is the measured value.

Table 2. Comparison of acceleration values.

Measure Point	A1			A2		
Data Type	**Max**	**Min**	**Mean in Time Frame**	**Max**	**Min**	**Mean in Time Frame**
Calculated value c_a (m/s^2)	4.282	−3.996	1.427	3.862	−3.776	1.486
Measured value μ_a (m/s^2)	4.708	−4.382	1.354	4.303	−4.137	1.529
Relative Error γ_a	9.05%	8.81%	5.39%	10.25%	8.73%	2.81%

From Table 2, we can find that the maximum relative errors of maximum and minimum values was 10.25%, while the relative errors of two mean values in the time frame were less than 6%, and this value of measure point A2 was even less than 3%. Compared with the maximum value or minimum value, which appeared only once in the whole time frame, the mean acceleration value in time frame can describe the actual vibration of tank walls better [23], therefore the model accuracy in acceleration calculation was acceptable.

Then starting at 60 ms, four procedure plots in the time domain were selected to verify the acoustic propagation process over time.

From Figure 5a, which is the plotting at 70 ms, we found that the elliptic front of the sound pressure had not reached the zone boundary on this plotting plane and it was centered around the power transformer. The contours distributed relatively uniformly and the sound pressure level decreased in sequence from 93.89 dB to 47.71 dB from the nearest length to the most distant length. Figure 5b,c are drawn at 80 ms and 90 ms respectively. The sound pressure generated by the power transformer reached the zone boundaries and gradually filled the total space. Particularly, acoustic reflections were observed as a distortion of contour lines in these two directions. In the Figure 5d drawn at 100 ms, further distortion of contour lines showed the result of superposition about the reflected wave and incident wave, and except part zonal regions, the sound pressure level stabilized around 85 dB at most area on this plane, this value coincided with field measured values well.

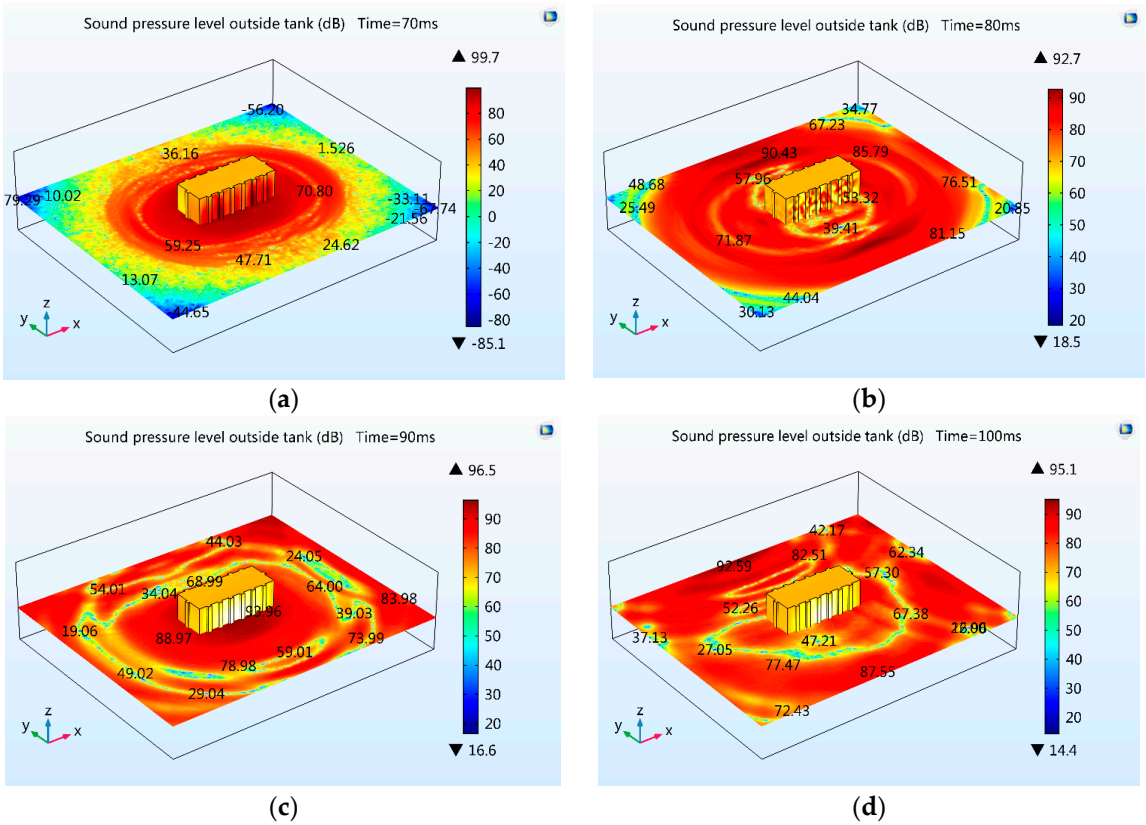

Figure 5. Sound pressure level outside tank at different time: (**a**) 70 ms; (**b**) 80 ms; (**c**) 90 ms; (**d**) 100 ms.

From the screenshots of generation, transmission, reflection and superposition, these four images in Figure 5 shows the representative moments during power transformer noise formation process from the view of sound pressure level in time domain. This computed results agree with the actual physical process well and the calculated sound pressure level is accordant with the measured values.

3.2. Verification in Frequency Domain

In the frequency domain, the main validation index is the sound pressure level at different frequencies. The position of the microphones around the oil tank are shown in Figure 4b by the four blue arrows. On this measurement plane, microphones are located at the height of the horizontal middle line of insulation oil tank, 1620 mm, the distance from Positions 1 and 3 to the nearest tank wall is 800 mm, the distance from Positions 2 and 4 to the nearest tank wall is 500 mm.

After field data acquisition, Fast Fourier transformation was used in both data processing about the measured value and numerical computation process in the model, to facilitate comparison between two sets of values. In consider of the lower frequencies less than 600 Hz take up a large proportion [24], 600 Hz is chosen as the upper limit frequency of 100 Hz, 200 Hz, 300 Hz, 400 Hz, and 600 Hz. The comparison between measured sound pressure values and calculated sound pressure values was shown in Table 3. We defined the percent average error, *Pae*, to characterize the accuracy of calculation. This value in table can be calculated according to the following formula:

$$Pae = \frac{\sum_{p=1,2\ldots}^{q} \left(\frac{|c_p - \mu_p|}{\mu_p} \times 100\% \right)}{q} \tag{13}$$

In Equation (13), *Pae* is the percent average error of a certain measure point, q is the frequency number of this measure point, c_p is calculated value from model, μ_p denotes the measured value.

Table 3. Comparison of sound pressure level values.

Frequency (Hz)		100		200		300		400		600		
Data Type		C_s	μ_s	C_s	μ_s	C_s	μ_s	C_s	μ_s	C_s	μ_s	Pae
Measuring Point and Data (dB)	①	63.46	68.02	62.82	64.25	50.82	59.16	46.58	40.54	51.82	51.82	7.59%
	②	62.12	69.06	53.27	64.62	49.58	50.08	43.00	40.54	46.56	49.06	7.96%
	③	64.97	71.82	63.04	64.62	59.65	56.93	42.57	37.02	37.02	43.04	9.15%
	④	64.37	71.50	62.06	68.26	51.50	47.90	45.06	40.54	44.97	49.06	9.21%

From Table 3, it can be found that the calculated sound pressure level distribution at each frequency were in accord with the actual measurement results, which means the sound pressure level generated by 100 Hz is greater than any other frequency of each measuring point for the reason that both the magnetostriction vibration frequency and the main frequency of the winding vibration are 100 Hz in 50 Hz power grid. For the percent average error, the maximum *Pae* value is 9.21% of measuring point four and the minimum *Pae* values is 7.59% belongs to point one. Calculation shows the average values of four *Pae* values is 8.48%, corresponding decibels value is 4.60 dB, so the error margin of this spatial acoustic radiation model in frequency meets the requirements. Combined verification in time and frequency domain above, we can conclude that the overall computational accuracy of the multi-physical field coupling method and model are satisfactory, and they can be used in spatial acoustic radiation characteristics analysis for an oil-immersed power transformer.

4. Analysis and Discussion

After the verification, this acoustic radiation model was used in multiple operating conditions to analyze the relevant acoustic radiation characteristics of the power transformer in its operation.

To ensure the commonality of this model, only acoustic impedance of ground surface was included, that is to say, in this section, and this model was placed in an open and flat terrain.

The analysis in multiple operating conditions were accomplished by two progressive steps. The first is the far-field analysis in the horizontal to obtain the effect of power transformer noise on specific frequencies at a certain distance. Secondly, directivity analysis in two vertical planes was used to collect spatial information across frequencies further, which formed the basis for the acoustic wave propagation characteristics of the power transformer could be presented.

Considering three phases load of most power transformers are almost balanced but load-rate levels may be different [25], here three kinds of different but balanced loads situations were set in front part of Table 4 from Situation (1) to Situation (3), therefore, L.R. is the shortened form of Load Rate and the same below. Then, three phase unbalanced loads may also exist in weak power grid structure area and may occur in temporary operation with fault, or during the process of power distribution networks reconfiguration in certain areas [26,27]. The acoustic radiation characteristics

analysis of power transformers in these extreme situations are hence essential for operators to release timely information, and then to reduce complaints from neighboring residents. So, two progressive unbalanced load situations were set in the lower part of Table 4 as Situation (4) and Situation (5).

Table 4. Multiple operating conditions.

Situation	Phase A	Phase B	Phase C
(1) L.R. 65%	65%	65%	65%
(2) L.R. 95%	95%	95%	95%
(3) L.R. 35%	35%	35%	35%
(4) L.R. S1	65%	95%	65%
(5) L.R. S2	65%	95%	35%

In situation (1) of Table 4, the tri-phase secondary winding currents are 65 percent of the secondary rated current, which gives consideration to both electric network security and economical operation [28], was set as the reference situation. Situation (2) is the heavily load situation, meaning that the power transformer is running closer to full capacity. This situation may exist at weak nodes of power grid especially during the summer or winter peak demand for electricity. Situation (3) stands for the low load situation, it exists in few regions and leaves a safety operation margin for reconfiguration of electric networks in emergency situations. In two unbalanced load situations, Situation (4) is used to describe the load increase of a certain phase, and it was named as L.R. S1; Situation (5), L.R. S2, is a more extreme case in that the load in one phase increased while the load of another phase decreased.

4.1. Far-Field Analysis

Far-field analysis about sound pressure level could show the direct effect of power transformer noise on the surrounding acoustic environment. As shown in Figure 6a, a horizontal plane at a height of 1620 mm above ground was selected as the drawing plane. In this plane, the increasing X direction was set as the reference direction and the counter-clockwise direction was chosen as the increasing direction of polar angle in polar diagram. Correspondingly, the increasing Z direction in vertical plane was selected as the normal direction. Combining the actual dimension of an 110 kV power substation and the general distance between the power transformer and surrounding buildings [29], 20 m was set as the assessment distance of far-field sound environment and 360 was set as the angle resolution.

Analysis results of far-field sound pressure level at different frequencies were shown in Figure 6b–f.

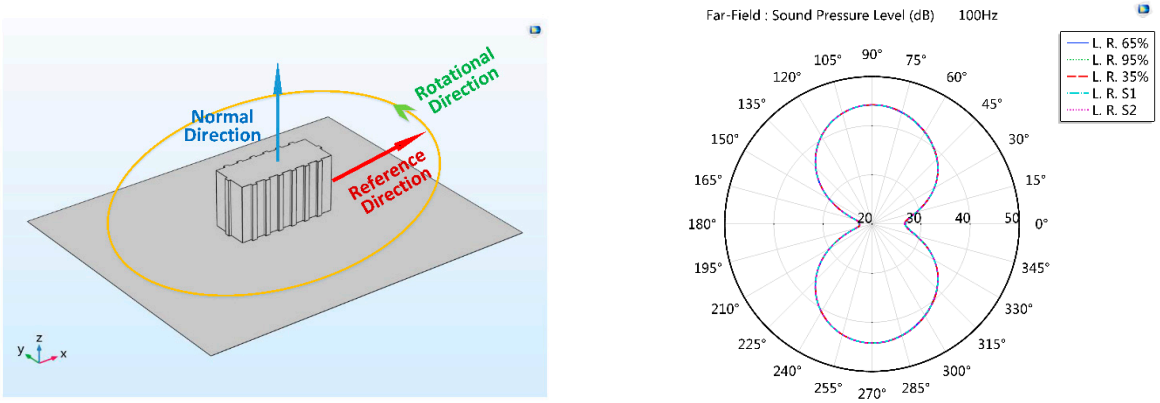

(**a**) (**b**)

Figure 6. *Cont.*

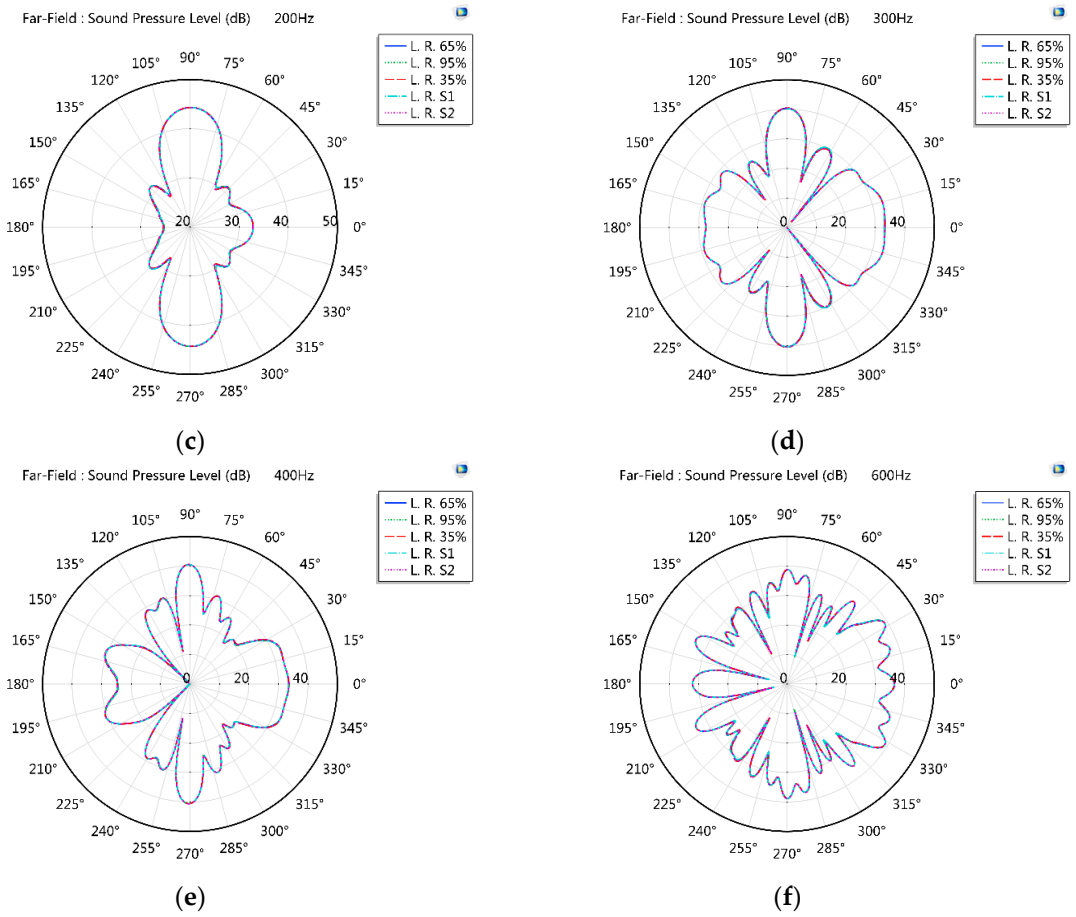

Figure 6. Reference plane of far-field analysis and results at different frequencies: (**a**) Sketch of the reference plane; (**b**) Sound pressure level of 100 Hz; (**c**) Sound pressure level of 200 Hz; (**d**) Sound pressure level of 300 Hz; (**e**) Sound pressure level of 400 Hz; (**f**) Sound pressure level of 600 Hz.

Through comparison of these five figures, we found the following relations:

1. At a certain frequency, along with the increase of polar angle, the changing trends about the sound pressure level of different load rate are almost accordant, at the same time, the slight differences at certain angles exists. For example, at the frequency of 200 Hz, the sound pressure level values of load rates of 35% at 55 degrees, 123 degrees, 237 degrees and 305 degrees, are slightly less than the corresponding values of the other four load rate situations. Similar difference also exists in 400 Hz situation as shown in Figure 6e, among the values at 135 degrees.
2. With increasing frequency, the progressively smaller wavelengths compared to the size of the power transformer makes the sound pressure level response gradually non-uniform: the graph of 100 Hz in Figure 6b can be roughly regarded as two crossed ellipses, while the graph shape of 600 Hz in Figure 6f is more irregular, but the five graphs are almost symmetrical along the 0 to 180 degree axis.
3. The maximum sound pressure level in the 45 degree sector region on both sides of the X directions are less than the values in corresponding regions on both sides of the Y directions. The difference are particularly obvious in the situations of 100 Hz and 200 Hz, in which the differentials are even greater than 20 dB.
4. In five far-field figures, along with the *x*-axis, the sound pressure levels in the 45 degree sector region on both sides of increasing X direction are overall greater than the corresponding values of decreasing X directions. The differential of these two values on the same diameter is greater than 3 dB or more.

4.2. Directivity Analysis

The above far-field analysis above was limited in a horizontal plane. In order to obtain more comprehensive spatial sound environment information around power transformer and get the spatial sound pressure level response versus frequency, directivity analysis in two mutually perpendicular vertical planes was implemented as planned in this section.

For the drawing parameters setting, as shown in Figure 7a, the YZ plane was set as the drawing plane, with the increasing X direction chosen as the normal direction and the increasing Z direction selected as the reference direction. In order to get the sound pressure level in ZX plane, the decreasing Y direction was selected as the normal direction in Figure 7b. Considering there are pebbles and sand in the sand pit below the power transformer in the substation, only the upper area above oil tank was selected as the calculating area, and the assessment distance was also 20 m.

After calculations, directivity plots about two planes were obtained as Figure 7c–l. In order to read data easily, corresponding values of contours were marked in appropriate regions.

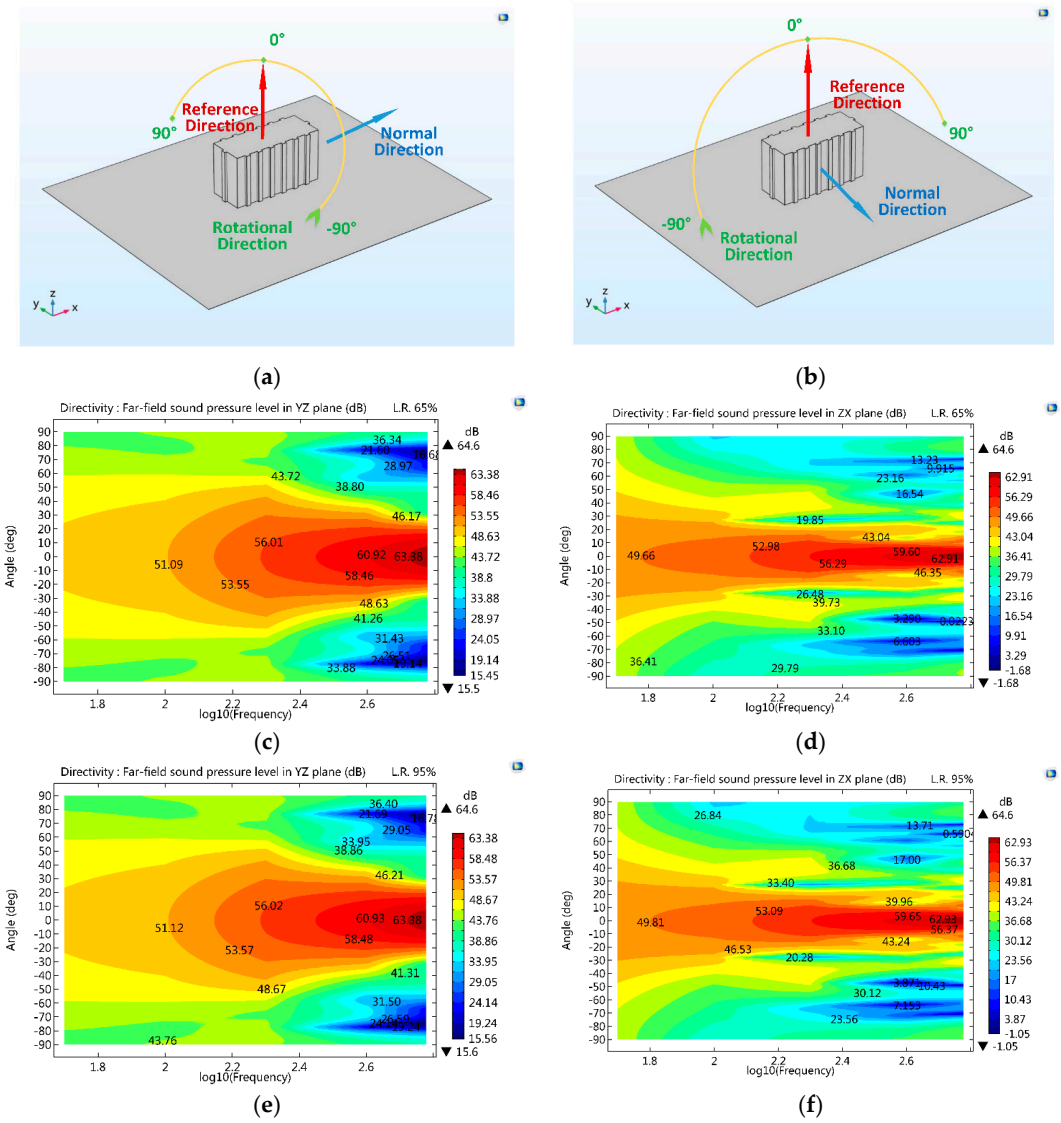

Figure 7. *Cont.*

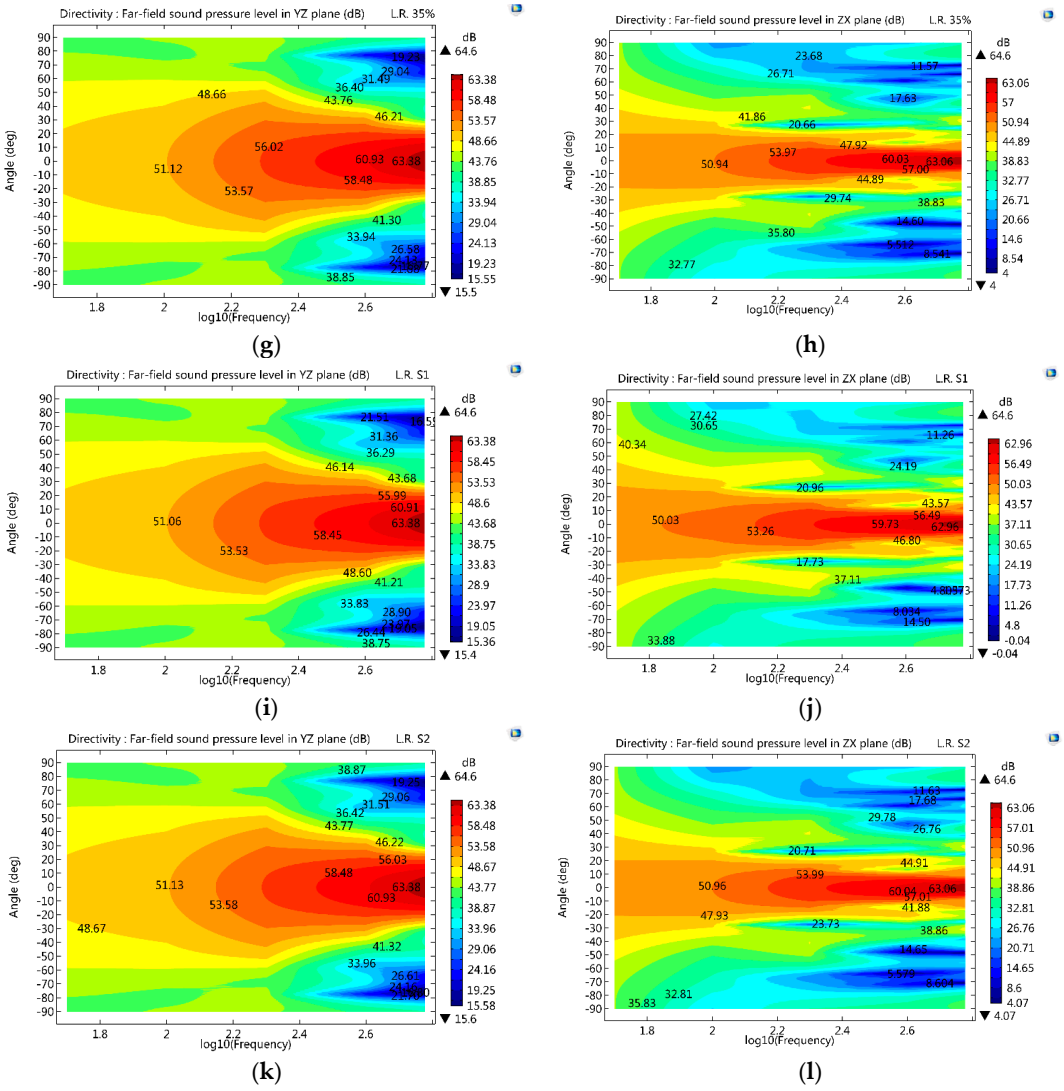

Figure 7. Reference plane of directivity analysis and results of different load rates: (**a**) Sketch of YZ plane; (**b**) Sketch of ZX plane; (**c**) Sound pressure level in YZ plane of L.R. 65%; (**d**) Sound pressure level in ZX plane of L.R. 65%; (**e**) Sound pressure level in YZ plane of L.R. 95%; (**f**) Sound pressure level in ZX plane of L.R. 95%; (**g**) Sound pressure level in YZ plane of L.R. 35%; (**h**) Sound pressure level in ZX plane of L.R. 35%; (**i**) Sound pressure level in YZ plane of L.R. S1; (**j**) Sound pressure level in ZX plane of L.R. S1; (**k**) Sound pressure level in YZ plane of L.R. S2; (**l**) Sound pressure level in ZX plane of L.R. S2.

According to directivity plots above, following items could be obtained:

1. The impact of changing load rate on the far-field sound pressure level in a particular series of vertical planes can be observed through the values of contours, while the discrepancy is not obvious. For example, in the five ZX planes directivity plots, when the angle is 0 degrees, the 100 Hz sound pressure levels from Situation (1) to Situation (5) respectively are 49.66 dB, 49.81 dB, 50.94 dB, 50.03 dB, and 47.93 dB, and the difference values are within 3.1 dB;
2. With the increase of frequency, the sound pressure levels in adjacent areas of 0 degrees concurrently increased, and these adjacent areas in the YZ planes (±20 degree along the 0 degree axis) are larger than the adjacent areas in ZX planes (±20 degree along the 0 degree axis), while the sound pressure level in other regions decreased with the increasing of frequency;

3. The directivity plots in YZ planes owns axial symmetry generally, but in ZX planes the directivity plots are asymmetrical, specifically, at the same frequency, the sound pressure level in the range from 60 degrees to 90 degrees is greater than the corresponding values in the range from −60 degrees to −90 degrees.

4.3. Discussion

Combined with the findings of above analysis, the reasons resulting to these differences were discussed from the following three aspects.

First, due to the adequate safety design to resist the attack of short-circuit current, the impact of changed winding currents caused by changed load on the vibration transmission process is existent but limited. Additionally, as the rated flux density inside transformer core is 1.68 T, which is between 1.5~1.8 T, the vibration amplitude of windings and tank wall (including magnetic shielding, etc.) caused by the leakage flux of load current is much smaller than the vibration amplitude caused by the magnetostriction of silicon steel sheets [30], so the impact of changed load rate on the far-field sound pressure level exists, while the discrepancy is not obvious.

Second, as shown in Figure 4b, for the asymmetric design of the internal structure in the oil tank and using the tank as a frame of reference, the core is not symmetrical along the YZ plane, so two symmetric points along the YZ plane on the tank obtained different vibrational energy from the first energy transmission path mentioned above, then it leads to the asymmetry about the external acoustic field of power transformer under load conditions in open and flat terrain.

Third, still from using the tank as a frame of reference, the core, windings and tank are symmetrical along the ZX plane, while for the different geometrical size and structural strength of adjacent tank lateral walls, at a certain frequency, the sound field in corresponding areas excited by tank vibration are discrepant.

So, under the good condition of clamps inside the tank, and ignoring the flux leakage, asymmetric internal structure, different geometrical size, and structural strength of adjacent tank lateral walls are the main reasons resulting to the specific acoustic radiation characteristics of power transformer in running.

5. Application

In this section, the application of quantitative analysis results above in reducing the influence of power transformer noise was discussed.

Under the good condition of clamps inside tank, the impact of changed load rate on the acoustic radiation characteristics was not obvious, so only reference situation in Table 4 was selected as the analysis object. In order to visualize the spatial acoustic radiation characteristics, the 3D far-field sound pressure level drawings combined the far-field sound pressure level plotting in the horizontal plane, and the directivity plotting in the vertical plane was accomplished and shown in Figure 8.

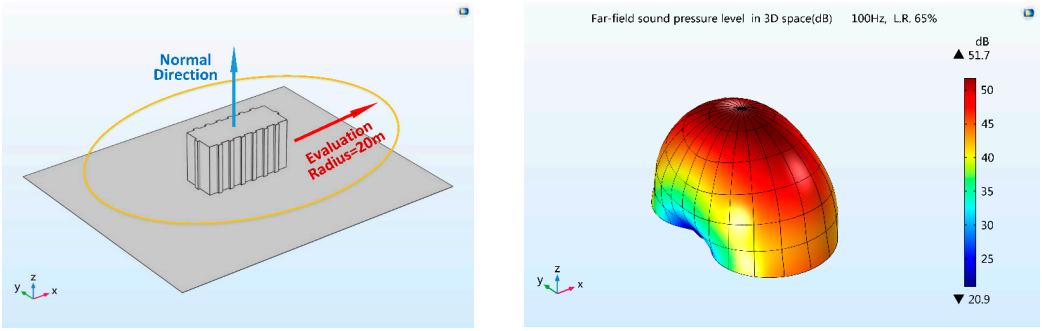

(**a**) (**b**)

Figure 8. *Cont.*

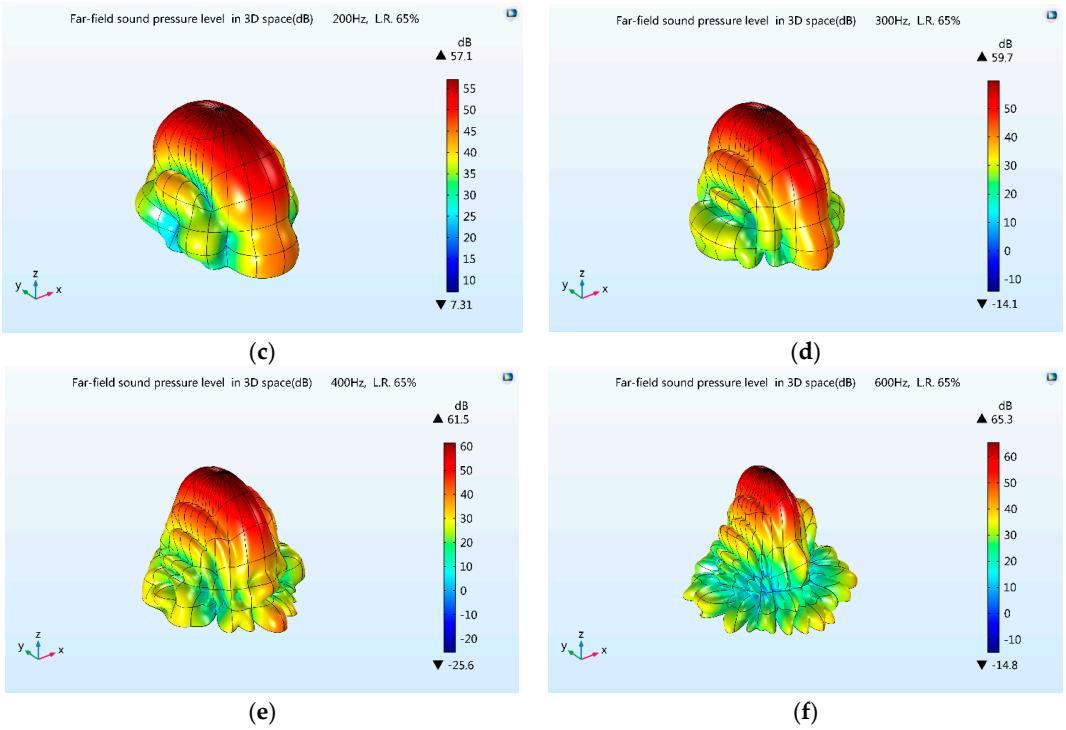

Figure 8. Distribution of sound pressure level in three-dimensional (3D) space at different frequencies of 65% load rate and the sketch of the reference plane: (**a**) Sketch of the reference plane; (**b**) Far-field sound pressure level in 3D space of 100 Hz; (**c**) Far-field sound pressure level in 3D space of 200 Hz; (**d**) Far-field sound pressure level in 3D space of 300 Hz; (**e**) Far-field sound pressure level in 3D space of 400 Hz; (**f**) Far-field sound pressure level in 3D space of 600 Hz.

So, to reduce the influence of power transformer noise, during the planning and design, the analysis result of acoustic radiation characteristics about power transformer could be applied in the following areas:

1. The far-field sound pressure level in the regions beside two long sides of oil tank are greater than the sound pressure level in the regions beside two short side, especially at 100 Hz and 200 Hz as shown in Figure 8b,c, so for the new buildings being planned around the substation, the designer should bypass the regions adjacent to the two long sides, or use them only for commercial construction; while for the positioning selection of sound proof walls inside substation, regions beside two long sides would be preferred locations.
2. In the region beside one short side of the oil tank which is closer to the core, the sound pressure level is higher than the sound pressure level at the opposite side at certain frequencies, so during the new building site selection in the power substation, this area should be excluded to reduce the reflective noise.
3. As shown in Figure 8b–f, the sound pressure level above oil tank grows with the frequency increase while in the region around the tank side wall, the sound pressure level decreases with the frequency increase.

So, for the building design around power substation, the designer should enhance the sound insulation design around high frequencies of noise for the upper part of the building, while for the lower part of the building, sound insulation design around the lower frequencies of noise should be strengthened.

6. Conclusions

With an aim for analyzing the spatial acoustic radiation characteristics of oil-immersed power transformers in running and applying them in reducing the noise influence, based on the energy transfer mechanism and the corresponding multi-physical field coupling method, far-field analysis and directivity analysis were accomplished. Combined discussion and application, following conclusions were obtained:

1. Assuming the core clamp and windings clamps works well, the impact of changed power transformer load rate on the far-field sound pressure level exists, while the discrepancy is not obvious.
2. In the horizontal region around the power transformer, the distribution of sound pressure level in the far-field is asymmetrical. To reduce the noise influence, urban planners should bypass the regions beside the two long sides of the oil tank, or at least prevent residential usage.
3. For high-rise building design around the power substation, sound insulation design about high frequencies of noise for the upper part should be enhanced, while for the lower part, analogous designs aiming at low frequencies of noise should be strengthened.

Acknowledgments: This project is supported by the National Natural Science Foundation of China (51377123). The authors would also like to thank the Hubei Natural Science Foundation of China for the financial support under the award 2017CFB402.

Author Contributions: Professor Liming Ying provided idea, designed the task flow and proofread the version to be published. Doctor Candidate Donghui Wang transformed idea into specific steps, completed the work of numerical experimental design, data analysis and interpretation and drafted the article. Jinwei Wang and Guodong Wang finished text revising and program designing. Data collection at worksite and data processing were completed by Xiaowen Wu and Jiangtao Liu.

Conflicts of Interest: The authors declare no conflict of interest.

References

1. Abramic, A.; Kotsev, A.; Cetl, V.; Kephalopoulos, S.; Paviotti, M. A Spatial Data Infrastructure for Environmental Noise Data in Europe. *Int. J. Environ. Res. Public Health* **2017**, *14*, 726. [CrossRef] [PubMed]
2. Ehlert, K. Perceptions of public primary school teachers regarding noise-induced hearing loss in South Africa. *S. Afr. J. Commun. Disord.* **2017**, *64*, e1–e12. [CrossRef] [PubMed]
3. International Organization for Standardization (ISO). *Acoustics—Description, Measurement and Assessment of Environmental Noise*; ISO 1996-1:2016; ISO: Geneva, Switzerland, 2016.
4. Hsu, C.-H.; Lee, S.-L.; Lin, C.-C.; Liu, C.-S.; Chang, S.-Y.; Hsieh, M.-F.; Huang, Y.-M.; Fu, C.-M. Reduction of Vibration and Sound-Level for a Single-Phase Power Transformer With Large Capacity. *IEEE Trans. Magn.* **2015**, *51*, 1–4. [CrossRef]
5. Girgis, R.; Bernesjo, M. Contributions to Differences between On-Site and Factory-Measured Noise Levels of Power Transformers. *IEEE Trans. Power Deliv.* **2015**, *30*, 82–88. [CrossRef]
6. Mizokami, M.; Kurosaki, Y. Noise variation by compressive stress on the model core of power transformers. *J. Magn. Magn. Mater.* **2015**, *381*, 208–214. [CrossRef]
7. Shilyashki, G.; Pfützner, H.; Hamberger, P.; Aigner, M.; Kenov, A.; Matkovic, I. Spatial distributions of magnetostriction, displacements and noise generation of model transformer cores. *Int. J. Mech. Sci.* **2016**, *118*, 188–194. [CrossRef]
8. Zhu, L.; Yang, Q.; Yan, R.; Zhang, X.; Yang, Y. Research on Dynamic Vibration of Transformer with Wireless Power Transfer System Load. *IEEE Trans. Magn.* **2015**, *51*, 1–4. [CrossRef]
9. Jin, M.; Pan, J. Vibration characteristics of a disk-type winding simulated by coupled concentric rings. *Appl. Acoust.* **2016**, *101*, 104–114. [CrossRef]
10. Jin, M.; Pan, J. Vibration transmission from internal structures to the tank of an oil-filled power transformer. *Appl. Acoust.* **2016**, *113*, 1–6. [CrossRef]
11. Jing, Z.; Hai, H.; Pan, J.; Yanni, Z. Identification of the nonlinear vibration system of power transformers. *Meas. Sci. Technol.* **2017**, *28*, 015005. [CrossRef]

12. Liu, D.; Du, B.; Yan, M.; Wang, S. Suppressing Noise for an HTS Amorphous Metal Core Transformer by Using Microperforated Panel Absorber. *IEEE Trans. Appl. Superconduct.* **2016**, *26*, 1–5. [CrossRef]
13. Zhao, W.; Chen, L.; Zheng, C.; Liu, C.; Chen, H. Design of absorbing material distribution for sound barrier using topology optimization. *Struct. Multidiscip. Optim.* **2017**, *56*, 315–329. [CrossRef]
14. Sung, W.P.; Hu, S.; Chen, S.Y.; Zou, H.S.; Li, T.N.; Kao, J.C.M. Research on the application of active sound barriers for the transformer noise abatement. *MATEC Web Conf.* **2016**, *44*, 02059.
15. Fan, R.; Su, Z.; Cheng, L. Modeling, analysis, and validation of an active T-shaped noise barrier. *J. Acoust. Soc. Am.* **2013**, *134*, 1990–2003. [CrossRef] [PubMed]
16. Ertl, M.; Voss, S. The role of load harmonics in audible noise of electrical transformers. *J. Sound Vib.* **2014**, *333*, 2253–2270. [CrossRef]
17. Tanaka, H.; Yamashita, D.; Member, S.; Niimura, T.; Member, S.; Yokoyama, R. Transformer Noise Level Optimization based on Reverse Calculation Problem and Linear Programming. In Proceedings of the 2008 IEEE Power and Energy Society General Meeting—Conversion and Delivery of Electrical Energy in the 21st Century, Pittsburgh, PA, USA, 20–24 July 2008; pp. 1–7.
18. Girgis, R.S.; Garner, K.; Bernesjo, M.; Anger, J. Measuring no—Load and load noise of power transformers using the Sound Pressure and Sound Intensity methods—Part-I: Outdoors measurements. In Proceedings of the 2008 IEEE Power and Energy Society General Meeting—Conversion and Delivery of Electrical Energy 21st Century, Pittsburgh, PA, USA, 20–24 July 2008; pp. 1–8. [CrossRef]
19. Alves, J.; Silva, L.; Remoaldo, P. The Influence of Low-Frequency Noise Pollution on the Quality of Life and Place in Sustainable Cities: A Case Study from Northern Portugal. *Sustainability* **2015**, *7*, 13920–13946. [CrossRef]
20. Girgis, R.S.; Bernesjö, M.S.; Thomas, S.; Anger, J.; Chu, D.; Moore, H.R. Development of ultra-low-noise transformer technology. *IEEE Trans. Power Deliv.* **2011**, *26*, 228–234. [CrossRef]
21. Moses, A.J.; Anderson, P.I.; Phophongviwat, T. Localized Surface Vibration and Acoustic Noise Emitted From Laboratory-Scale Transformer Cores Assembled From Grain-Oriented Electrical Steel. *IEEE Trans. Magn.* **2016**, *52*, 1–15. [CrossRef]
22. Niu, W.; Li, N.; Chen, S.; Tang, S.; Hu, Y.; Cai, J.; Lv, L.; Jin, C.; Bai, Z.; Zhong, H. Experimental study of the evaporative cooling system in a low-noise power transformer. In Proceedings of the 2012 China International Conference on Electricity Distribution (CICED), Shanghai, China, 10–14 September 2012; Volume 8562, pp. 1–4.
23. Galbrun, L. Space averaging of vibration level differences measured in lightweight building structures. *Appl. Acoust.* **2011**, *72*, 205–209. [CrossRef]
24. He, Z.C.; Li, E.; Liu, G.R.; Li, G.Y.; Cheng, A.G. A mass-redistributed finite element method (MR-FEM) for acoustic problems using triangular mesh. *J. Comput. Phys.* **2016**, *323*, 149–170. [CrossRef]
25. International Electrotechnical Commission (IEC). *Power Transformers—Part 7: Loading Guide for Oil-Immersed Power Transformers*; IEC 60076-7:2005; IEC: Genevacity, Switzerland.
26. Teng, J.-H.; Liao, S.-H.; Leou, R.-C. Three-Phase Harmonic Analysis Method for Unbalanced Distribution Systems. *Energies* **2014**, *7*, 365–384. [CrossRef]
27. Seo, H.-C. New Adaptive Reclosing Technique in Unbalanced Distribution System. *Energies* **2017**, *10*, 1004. [CrossRef]
28. Biçen, Y.; Aras, F.; Kirkici, H. Lifetime Estimation and Monitoring of Power Transformer Considering Annual Load Factors. *IEEE Dielectr. Electr. Insul. Soc.* **2014**, *21*, 1360–1367. [CrossRef]
29. Pérez, E.I.; Rada, J.B. *Design and Costs Estimation of Electrical Substations Based on Three-Dimensional Building Blocks*; Springer: Berlin/Heidelberg, Germany, 2010; pp. 574–583.
30. Yucheng, X. *Power Transformer Manual*, 2nd ed.; China Machine Press: Beijing, China, 2014.